Peptide Models. 3. Conformational Potential Energy Hypersurface of Formyl-L-valinamide

Wladia Viviani,† Jean-Louis Rivail,† Andras Perczel,‡,§ and Imre G. Csizmadia*,†,§

Contribution from the Laboratoire de Chimie Théorique, U.A. 510 CNRS, Université de Nancy-I, BP 239, F-54506 Vandœuvre-les-Nancy, Cedex, France, Department of Organic Chemistry, Institute of Chemistry, Eötvös University, Budapest, Hungary, and Department of Chemistry, University of Toronto, Toronto, Ontario, Canada M5S 1A1

Received April 15, 1992

Abstract: Out of the 27 legitimate minima of the 3D Ramachandran map, $E = E(\phi,\psi,\chi^1)$, the existing 20 conformations of formyl-L-valinamide have been determined by *ab-initio* SCF-MO computations. In the *gauche* side-chain conformations ($\chi^1 = 60°$ and $\chi^1 = 300°$), the pattern of minima on the backbone potential energy surface, *i.e.* on the 2D Ramachandran map, $E = E(\phi,\psi)$, is equivalent to the backbone conformation of the corresponding L-alanine derivative, which shows the absence of the α_L and ϵ_L conformations. However, in the *anti* conformation ($\chi^1 = 180°$) an additional backbone conformation, the one labeled as δ_L, has disappeared. This implied that, at the $\chi^1 = 180°$ torsional angle, on the $E = E(\chi^1)$ potential curve crosssection, the δ_L conformation is destabilized to such a degree that the δ_L minimum is replaced by a higher indexed critical point ($\lambda = 1$) on the potential energy hypersurface of $3N-6$ independent variables. The β_L backbone conformation is also destabilized at $\chi^1 = 180°$ to a higher energy than either of the two nonequivalent *gauche* conformations; nevertheless, it remained a minimum. In contrast to the above, three backbone conformations (γ_L, γ_D, and α_D) are stabilized in the *anti* ($\chi^1 = 180°$) side-chain conformation with respect to the two nonequivalent *gauche* conformations. A new method has been developed for a unique energy partitioning in order to quantify the magnitude of the side chain/backbone interaction. The numerical values for such side chain/backbone interactions have been calculated for the ^{i}Pr group in the various backbone conformations of formyl-L-valinamide relative to that of hydrogen in the corresponding backbone conformations of formylglycinamide. The computations have clearly shown that even an apolar side chain was able to interact with the peptide backbone so drastically that it could annihilate one of the otherwise legitimate minima through an unfavorable backbone and side-chain torsional angles combination.

1. Introduction

1.1. Preamble. The β-sheet formation potential (*i.e.* formation probability) of valine is the highest of all amino acids.[1] For example pure polyvaline has a full β-sheet structure corresponding to a $(\beta_L)_n$ conformation. The helix formation potential of valine is average. In contrast to that, the global β-turn formation potential (averaging over the four possible positions of a β-turn) is the second or third worst of the 20 amino acids, superseded by the other two apolar amino acid residues: leucine and isoleucine.[1]

Consequently, protein conformation predicting methods (see for example ref 2) are not able to predict accurately backbone conformations of valine residues for β-turns, since they aim to predict primarily helices and sheets. It is not surprising, therefore, that peptides which include valine residues have not been studied extensively. Small peptides, such as Ac-Gly-NHMe, Ac-Ala-NHMe, For-Gly-NH_2 and For-Ala-NH_2 have been studied computationally within the *ab-initio* framework,[3-12] but no valine derivative has been studied in the same way.

Yet, valine enjoys a certain distinction among the amino acids. If all 20 amino acids were equally important, then statistically one would anticipate a 5% occurrence for each. Of course, such uniformity is not expected to be the case. Also, the percentage of occurrence may vary from protein to protein. For example, collagen has a considerably higher percentage of glycine, alanine, and proline residues than 5%; therefore, all other amino acids, including valine, have less than 5% occurrence. However, the relative occurrence of valine in *Escherichia coli* proteins is already 6%. Furthermore, a set of 78 selected proteins[13] had 860 valine residues out of a total of 11 793 residues, amounting to 7.3%. (The X-ray data of proteins[14,15] were taken from Brookhaven Protein Structure Databank (BPSD). Their stereochemical parameters such as the resolution, the R factor, and the core percentage were taken as recommended.[16])

There are only a few examples, in the literature, of X-ray-determined structures of small peptides containing valine. These include Ac-Val-NH_2 using both L-valine[17] and DL-valine[18] as well

† Université de Nancy-I.
‡ Eötvös University.
§ University of Toronto.

(1) Fasman, G. D. *Prediction of Protein Structure and the Principles of Protein Conformation*; Plenum Press: New York, 1989.
(2) Chou, P. Y.; Fasman, G. D. *J. Mol. Biol.* **1977**, *115*, 135–175.
(3) Sellers, H. L.; Schafer, L. *J. Am. Chem. Soc.* **1978**, *100*, 7728–7729.
(4) Schafer, L.; Sellers, H. L.; Lovas, F. J.; Suenram, R. D. *J. Am. Chem. Soc.* **1980**, *102*, 6566–6568.
(5) Schafer, L.; Van Alsenoy, C.; Scarsdale, J. N. *J. Chem. Phys.* **1982**, *76*, 1439–1444.
(6) Scarsdale, J. N.; Van Alsenoy, C.; Klimkowski, V. J.; Schafer, L.; Momany, F. A. *J. Am. Chem. Soc.* **1983**, *105*, 3438–3445.
(7) Schafer, L.; Klimkowski, V. J.; Momany, F. A.; Chuman, H.; Van Alsenoy, C. *Biopolymers* **1984**, *23*, 2335–2347.
(8) Klimkowski, V. J.; Schafer, L.; Momany, F. A.; Van Alsenoy, C. *J. Mol. Struct.* **1985**, *124*, 143–165.
(9) Head-Gordon, T.; Head-Gordon, M.; Frisch, M. J.; Brooks, C., II; Pople, J. A. *Int. J. Quantum Chem., Quantum Biol. Symp.* **1989**, *16*, 311–319.
(10) Perczel, A.; Ángyán, J. G.; Kajtár, M.; Viviani, W.; Rivail, J.-L.; Marcoccia, J.-F.; Csizmadia, I. G. *J. Am. Chem. Soc.* **1991**, *113*, 6256.
(11) Head-Gordon, T.; Head-Gordon, M.; Frisch, M. J.; Brooks, C., II; Pople, J. A. *J. Am. Chem. Soc.* **1991**, *113*, 5989–5997.
(12) Frey, R. F.; Coffin, J.; Newton, S. Q.; Ramek, M.; Cheng, V. K. W.; Momany, F. A.; Schafer, L. *J. Am. Chem. Soc.* **1992**, *114*, 5369.
(13) McGregor, M. J.; Suhail, I. A.; Sternberg, J. E. *J. Mol. Biol.* **1987**, *198*, 295–310.
(14) Bernstein, F. C.; Koetzle, T. F.; Williams, G. J. B.; Mayer, E. F., Jr.; Brice, M. D.; Rodgers, J. R.; Kennard, O.; Shimanouchi, T.; Tasumi, M. *J. Mol. Biol.* **1977**, *112*, 535–542.
(15) Allen, F. H.; Bergerhoff, G., Sievers, R. *Crystallographic Database-Information Content, Software System, Scientific Applications.* In *Data Commission of the International Union of Crystallography*; Abola, E. E., Bernstein, F. G., Bryant, S. H., Koetzle, T. F., Weng, J., Eds.; Bonn/Cambridge/Chester: 1987; pp 107–132.
(16) Morris, A. L.; MacArthur, M. W.; Hutchinson, E. G.; Thornton, M. J. *Proteins: Struct., Funct., and Genet.* **1992**, *12*, 345–364.
(17) Aubry, A.; Cung, M. T.; Marraund, M. *Cryst. Struct. Commun.* **1982**, *11*, 129–133.

0002-7863/93/1515-8321$04.00/0

Chart I

300°	γ_D	δ_D	α_L		300°	γ_D	δ_D	•
ψ 180°	ϵ_D	β_L	ϵ_L		ψ 180°	ϵ_D	β_L	•
60°	α_D	δ_L	γ_L		60°	α_D	δ_L	γ_L
	60°	180°	300°			60°	180°	300°
		ϕ					ϕ	

a. MDCA and MM surfaces b. ab-initio surface

Chart II

family type	side chain	example
1	H	glycine
2	CH_3	alanine
3	CH_2Q	serine
4	CHQ'Q''	valine

as a dipeptide derivative,[19] ^{t}BuOCO-Val-Ser-NHMe. Although very little is known about the valine backbone conformations, even less is known about its side-chain conformations.

For all these reasons the study of small peptides containing valine is of particular importance.

1.2. Scope. The interaction between side chain and backbone in peptides is a fundamental question that has not been answered satisfactorily as yet. Due to the rather large dipole moment of an amide plane, it is obvious that a polar side chain may have a backbone conformation influencing capacity, as was found for For-Ser-NH_2.[20] However an apolar side chain may also influence the topology of an $E = E(\phi,\psi,\chi)$ type potential energy hypersurface (PEHS). A 2D cross section of such a PEHS, $E = E(\phi,\psi,\chi)$, for any given χ values leads to a 2D Ramachandran map $E = E(\phi,\psi)$.

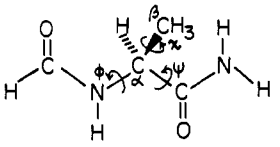

I

$E = E(\phi,\psi,\chi)$

The pattern of minima of the $E(\phi,\psi)$ potential surfaces[10] of compound **I** is shown in Chart I as obtained by multidimensional conformational analysis (MDCA) and molecular mechanics (MM) as well as *ab-initio* SCF computations.[10]

Clearly, in the case of compound **I** the α_L and ϵ_L legitimate conformations (as shown in Chart Ia) have disappeared from the *ab-initio* Ramachandran map (Chart Ib). The 19 common amino acid side chains (proline has no flexible side chain), which necessarily influence the $E(\phi,\psi)$ surface, can be divided into four groups, depending on the degree of substitution at the β-carbon (C^β) atom. With the lack of a C^β atom, glycine forms the sole example of the achiral family (cf. Chart II).

The present paper therefore deals with the last family type of Chart II, exemplified by formyl-L-valinamide (**II**), which is the simplest model compound of this group with Q' = Q'' = CH_3.

Here, energy is considered as the function of five independent conformational variables $E = E(\phi,\psi,\chi^1,\chi^2,\chi^3)$. However each of the two methyl groups have three degenerate torsional minima; therefore, the system may be described effectively with three independent torsional variables $E = E(\phi,\psi,\chi^1)$ when χ^2 and χ^3 are optimized but nominally $\chi^2 = \chi^3 = 60°$.

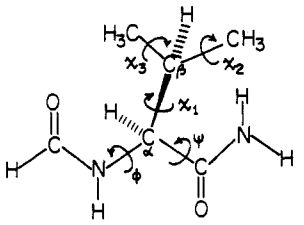

II

$E = E(\phi,\psi,\chi^1,\chi^2,\chi^3)$

The Newman projections, in which we are looking along the C^α–C^β bond, are shown in Chart III. Considering the two tertiary protons associated with C^α and C^β, we can refer to two nonequivalent *gauche* ($\chi^1 = 60°$ and $\chi^1 = 300°$) and one *anti* ($\chi^1 = 180°$) conformations (Chart III). This chart shows both the standard and the currently favored representation for the χ^1 values.

2. Method

2.1. Energy Computations. *Ab-initio* SCF calculations have been carried out using the GAUSSIAN-88[21] and the HONDO[22] programs at the 3-21G basis set level.[23] The geometries of stable structures were gradient optimized, and the optimization was stopped when all the gradients in internal coordinates were less than 5.0×10^{-4} a.u. All structures were fully optimized (along all the 60 internal coordinates), but in the present conformational analysis only the five selected torsional angles (ϕ, ψ, χ^1, χ^2, χ^3) are reported.

2.2. Energy Partitioning. Since amino acids differ from each other by the number of atoms they contain, their computed SCF energies cannot be compared directly. To bring them to the same energy scale, some arithmetical procedure, like the one introduced earlier,[24] is required. Such a procedure is based on the conformational energy decomposition into several contributions.

Considering simple amino acid diamides (AR), where the side chain R may be H (GLY), Me (ALA), and ^{i}Pr (VAL), the stabilization energy (E_x^{stabil}) of such an amino acid diamide AR in its optimized conformation x may be derived in two equivalent forms *via* methods A and B.

Method A. It is sometimes convenient to choose a fixed conformation as a reference state and measure the substituent effect with respect to this reference state. In this particular case the "reference state" means a "reference compound" (*i.e.* For-Gly-NH_2) in its "reference conformation" (*i.e.* its global minimum γ_L). In such a case a genuine isodesmic reaction may be constructed, as illustrated by Scheme I (the symbols used for the energy values are written below the molecular structure).

According to this equation the two reactants are in their global minimum energy conformation while one of the products could be in any one of its possible conformations x. In such a case, the overall energy of the reaction (E_x^{stabil}) gives us the energy value associated with the chemical change plus the energy associated with the conformational change of one of the products.

$$E_x^{stabil} = E_x^{AR} - [(E_0^{AH} - E_0^{MeH}) + E_0^{MeR}] \qquad (1)$$

The same E_x^{stabil} can be related to the conventional relative energy

(18) Aubry, A.; Marraund, M.; Protas, J.; Neil, J. *C. R. Acad. Sci. Paris* **1974**, *287c*, 163–166.

(19) Perczel, A.; Foxman, B. M.; Fasman, G. D. *Proc. Natl. Acad. Sci. U.S.A.* **1992**, *89*, 8210–8214.

(20) Perczel, A.; Daudel, R.; Ángyán, J. G.; Csizmadia, I. G. *Can. J. Chem.* **1990**, *68*, 1882.

(21) Frisch, M. J.; Head-Gordon, M.; Schlegel, H. B.; Raghavachari, K.; Binkley, J. S.; Gonzales, C.; Defrees, D. J.; Fox, D. J.; Whiteside, R. A.; Seeger, R.; Melius, C. F.; Baker, J.; Martin, R. L.; Kahn, L. R.; Steward, J. J. P.; Fluder, E. M.; Topiol, S.; Pople, J. A. *GAUSSIAN-88*; GAUSSIAN Inc.: Pittsburgh, PA, 1988.

(22) Dupuis, M.; Watts, J. D.; Villar, H. O.; Hurst, G. J. B. *QCPE Bull.* **1982**, *8* (2), 79–82.

(23) Binkley, J. S.; Pople, J. A.; Hehre, W. J. *J. Am. Chem. Soc.*, **1980**, *102*, 939.

(24) Viviani, W.; Rivail, J. L.; Csizmadia, I. G. *Theor. Chim. Acta* **1993**, *85*, 189–197.

Chart III

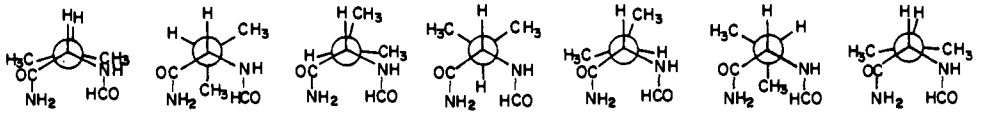

χ_1	0°	60°	120°	180°	240°	300°	360°
χ_1^{STD}	0°	-60°	-120°	-180° +180°	+120°	+60°	0°

Scheme I

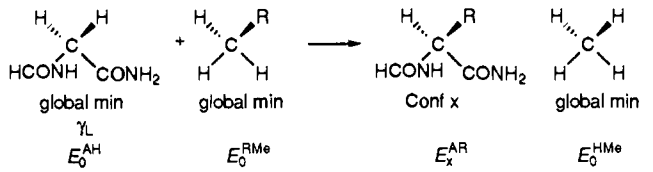

$$\Delta E_x^{AR} = E_x^{AR} - E_0^{AR} \quad (2)$$

by the following expression:

$$E_x^{stabil} = \Delta E_x^{AR} + [E_0^{AR} - (E_0^{AH} - E_0^{MeH} + E_0^{MeR})] \quad (3)$$

Method B. The quantity E_x^{stabil} can also be deduced from the four energy components described below: (1) E_{dist}^{AH} is the energy value associated with the conformational change (*distortion*) when going from the global minimum of AH toward the geometry assumed in conformation x of AR. Therefore,

$$E_{dist}^{AH} = E_x^{AH} - E_0^{AH} \quad (4)$$

(2) E_{dist}^{RMe} corresponds to a geometry in which the only optimized parameters are the length of the two C–H bonds created by replacing the HCONH and the $CONH_2$ groups of conformation x of AR by two H atoms

$$E_{dist}^{RMe} = E_x^{RMe} - E_0^{RMe} \quad (5)$$

(3) E_{dist}^{HMe} is defined in an analogous way, as

$$E_{dist}^{HMe} = E_x^{HMe} - E_0^{HMe} \quad (6)$$

(4) $E_x^{(SC/BB)int}$ is the quantification of the interaction energy between backbone and side chain.

$$E_x^{(SC/BB)int} = E_x^{AR} - [(E_x^{AH} - E_x^{MeH}) + E_x^{MeR}] \quad (7)$$

It is easy to verify that the quantity

$$[(E_x^{AH} - E_x^{MeH}) + E_x^{MeR}] \quad (8)$$

corresponds to the energy of a given amino acid diamide, in the absence of such interaction. Thus, subtracting this quantity from the energy of the original amino acid diamide E_x^{AR}, one obtains the value of side chain/backbone interaction at conformation x. By combining those terms with eq 1, we obtain

$$E_x^{stabil} = E_x^{(SC/BB)int} + E_{dist}^{AH} + E_{dist}^{MeR} - E_{dist}^{MeH} \quad (9)$$

E_x^{stabil} is now presented as the sum of the various energy contributions existing inside the molecule.

3. Results and Discussion

Interactions within proteins can be divided into four categories: (i) backbone interactions, (ii) backbone/side chain interactions, (iii) nearest neighbor interactions, and (iv) long-range interactions. For long-range interactions (iv) one must study at least a long peptide if not the whole molecule. All nearest neighbor interactions (iii) should be present in tripeptide derivatives (*i.e.* tetramides), but most of these interactions would manifest themselves in dipeptide derivatives (*i.e.* triamides). In contrast to the above, the smallest unit, the diamide derivative of a single amino acid, such as HCONH–CHR–$CONH_2$, is expected to reveal most of the features of i and ii.

Although the space available for the R group might be slightly different in proteins than it is in the simple diamides, an understanding of the conformational intricacies of these amino acid diamides is absolutely essential before the whole problem might be deciphered. In the present paper the results obtained for the diamide of L-valine (R = $(CH_3)_2CH$) are compared to those of L-alanine (R = CH_3) and glycine (R = H) derivatives.[10]

3.1. Topology of the PEHS. Table I reports the conformations and energies (as well as the length of the gradient vectors of the full optimization) of these 20 minima, that could be found on the potential energy hypersurface (PEHS) of $E = E(\phi,\psi,\chi^1,\chi^2,\chi^3)$. Since each of the two CH_3 groups of the isopropyl substituent, $C^\beta H(CH_3)_2$, can have only one unique minimum, it is enough to study the characteristics of the simpler problem specified by the following potential energy hypersurface (PEHS)

$$E = E(\phi,\psi,\chi^1) \quad (10)$$

with the implicit assumption that χ^2 and χ^3 are optimized.

Each of the three torsional angles (ϕ, ψ, and χ^1) are expected to have three minima;[10] therefore, on the basis of MDCA[25] one would expect to find $(3 \times 3) \times 3 = 27$ minima. However even in the case of the L-alanine derivative, the α_L and ϵ_L conformations disappear,[10] suggesting the existence of $(3 \times 3 - 2) \times 3 = 7 \times 3 = 21$, rather than 27, minima for the valine derivative (**II**). In addition, at the nominal value of $\chi^1 = 180°$, the δ_L conformation has also disappeared as a minimum, since it turned out to be a higher indexed critical point ($\lambda = 1$). This implied the loss of not six but a total of seven minima, which accounts for the observation of only 20 rather than 27 minima.

3.2. Energetics of the PEHS. It is interesting to compare the energy spectrum of the various minima for formylglycinamide and formyl-L-alaninamide reported earlier[10] with the energy values associated with the various minima of formyl-L-valinamide. The minima for the glycine, alanine, and valine derivatives were found within the 4.5, 8.5, and 12.5 kcal/mol range, respectively. A detailed correlation diagram is given in Figure 1. This figure indicates that the larger the substituent the more extensive is its interaction with the backbone, since the spectra of the appropriate energy levels are spread out more and more as substitution goes from H through CH_3 to $CH(CH_3)_2$. However, this figure should not be interpreted to mean that the larger the R group the greater is its destabilizing effect (see discussion later). It should be noted that the relative energy order between different backbone minima is maintained in all cases with only one exception. It concerns the reversal of stability between β_L and γ_D for the valine derivative in the *anti* ($\chi^1 = 180°$) side-chain conformation.

(25) (a) Csizmadia, I. G. General and Theoretical Aspects of the Thiol Group. In *The Chemistry of the Thiol Group*; Patai, S., Ed.; The Chemistry of Functional Groups; John Wiley and Sons: New York, 1974; pp 1–109 (cf. particularly pages 36–41 including Figures 23 and 24 as well as Table 20). (b) Csizmadia, I. G. Multidimensional Stereochemistry and Conformational Potential Energy Topology. In *New Theoretical Concepts for Understanding Organic Reactions*; by Bertrán, J., Ed.; Reidel Publishing Co.: Dordrecht, The Netherlands, 1989; pp 1–31.

Table I. Characteristics of Minima ($\lambda = 0$), Gradient Optimized at the HF/3-21 Basis Set Level of Theory, for Formyl-L-valinamide

symbol	ϕ_{std}[a]	ψ_{std}[a]	ϕ_{top}[a]	ψ_{top}[a]	χ^2[b]	χ^2[b]	χ^3[b]	E[c]	ΔE[d]	g[e]
α_D	49.990	43.108	49.990	43.108	75.110	56.233	63.099	−490.101 076	8.69	1.9
α_D	60.197	40.939	60.197	40.939	196.423	63.890	61.886	−490.104 167	6.75	4.6
α_D	47.227	44.565	47.227	44.565	298.707	52.284	64.403	−490.102 413	7.85	1.2
α_L					no optimum found					
α_L					no optimum found					
α_L					no optimum found					
β_L	−162.317	156.772	197.683	156.772	64.242	53.580	64.709	−409.111 766	1.98	3.5
β_L	−136.016	142.837	223.984	142.837	186.010	65.625	62.229	−490.109 591	3.35	4.8
β_L	−141.613	163.683	218.387	163.683	293.281	55.207	65.486	−490.112 050	1.81	4.0
γ_D	62.885	−39.198	62.885	320.802	84.168	63.654	66.933	−490.106 581	5.24	0.8
γ_D	73.972	−61.005	73.972	298.995	178.006	58.679	56.558	−490.111 417	2.20	2.6
γ_D	59.588	−38.618	59.588	321.382	311.259	57.974	66.705	−490.105 984	5.61	2.1
γ_L	−84.995	66.121	275.005	66.121	63.134	55.160	59.939	−490.113 864	0.67	4.1
γ_L	−83.332	71.645	276.668	71.645	185.726	60.403	59.828	−490.114 927	0.00	4.3
γ_L	−84.988	63.181	275.012	63.181	293.128	53.565	62.809	−490.114 353	0.36	2.5
ϵ_D	76.167	162.345	76.167	162.345	102.286	55.259	66.558	−490.095 239	12.35	4.8
ϵ_D	75.090	152.769	75.090	152.769	181.850	61.003	58.510	−490.097 836	10.72	0.2
ϵ_D	70.889	170.577	70.889	170.577	327.319	62.184	72.157	−490.097 303	11.06	4.7
ϵ_L					no optimum found					
ϵ_L					no optimum found					
ϵ_L					no optimum found					
δ_D	−176.209	−33.786	183.791	326.214	65.290	60.253	67.268	−490.102 275	7.94	3.0
δ_D	−137.568	−60.129	222.432	299.871	187.733	66.730	64.288	−490.100 560	9.02	3.8
δ_D	−169.949	−46.888	190.051	313.112	261.131	54.361	59.458	−490.097 576	10.89	1.4
δ_L	−134.148	35.309	225.852	35.309	71.228	56.621	64.564	−490.108 179	4.23	4.2
δ_L					no optimum found					
δ_L	−123.742	28.360	236.258	28.360	298.771	58.193	65.693	−490.109 674	3.30	3.8

[a] The standard (std) and topologically (top) useful (ϕ,ψ) angle pairs are defined in ref 10. [b] Side-chain torsional angles specified in structure II. [c] Hartrees. [d] kcal/mol. Relative stability with respect to γ_L at $\chi^1 = 180°$. [e] Gradient length in units of 10^{-4} a.u.

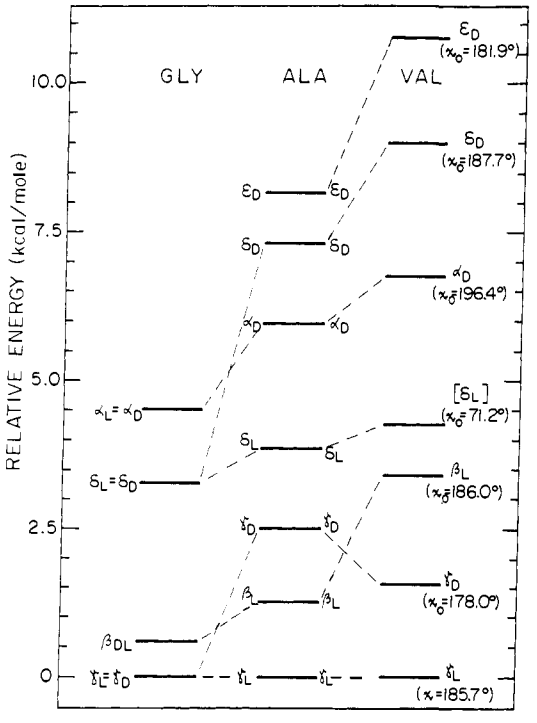

Figure 1. Comparison of relative stabilities of formyl amino acid amide derivatives for glycine (GLY), alanine (ALA), and valine (VAL) on the basis of *ab-initio* calculations.

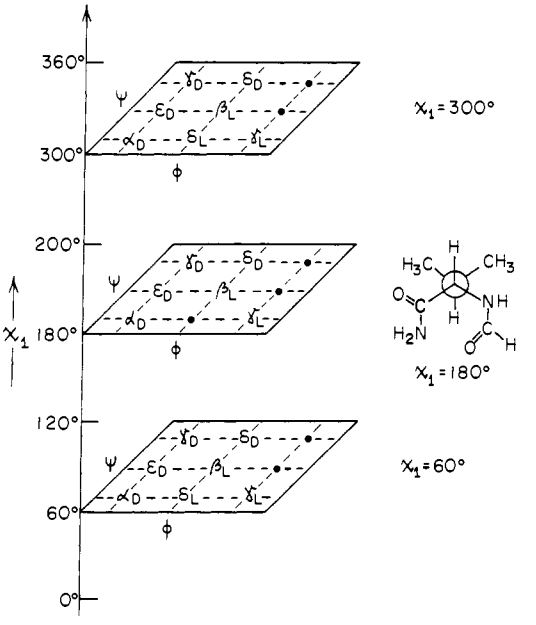

Figure 2. Schematic illustration of the pattern of the three-dimensional Ramachandran map, $E = E(\phi,\psi,\chi^1)$ computed for formyl-L-valinamide.

Considering the question of the potential energy hypersurface of formyl-L-valinamide, the pattern of such a three-dimensional Ramachandran map is schematically depicted in Figure 2. Note that at $\chi^1 = 60°$ and $\chi^1 = 300°$ the topology of the PES looks like that of formyl-L-alaninamide, with missing α_L and ϵ_L conformations.[10] In contrast, at $\chi^1 = 180°$ the pattern of the formyl-L-valinamide backbone conformations is slightly different as the δ_L conformation is annihilated, since it turned out to be a higher indexed critical point. Projecting these three topologies of Figure 2 on one plane and also marking the location of the minima of formylalaninamide (marked by open circles) and formylglycinamide (marked by open squares) together with the topology of the ideal surface (marked by open asterisks), one obtains Figure 3. This figure indicates that each of these families of points falls within a relatively small domain, denoted by an ellipse, in the vicinity of the ideal conformation. The molecular structures for the various *anti* conformation ($\chi^1 = 180°$) are shown in Figure 4, in an arrangement that is analogous to the pattern of the two-dimensional Ramachandran map.

A correlation diagram (Figure 5) in which the characteristic minima with varying χ^1 values are compared is even more revealing. Ignoring the δ_L conformation, as it has no minimum at $\chi^1 = 180°$, we may make a number of observations. In the δ_D backbone conformation there is a monotonic increase in energy while the ϵ_D backbone conformation there is a monotonic decrease in energy as one goes from $\chi^1 = 60°$ through $\chi^1 = 180°$ to χ^1

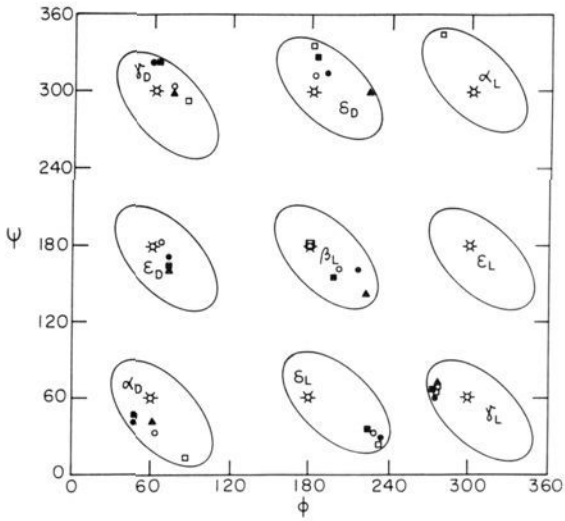

Figure 3. Scatter of points on the two-dimensional Ramachandran map, $E = E(\phi,\psi)$, including formylglycinamide (open squares), formyl-L-alaninamide (open circles), and formyl-L-valinamide at $\chi^1 = 60°$ (solid squares), $\chi^1 = 180°$ (solid triangles), and $\chi^1 = 300°$ (solid diamonds) in relation to the ideal conformation (open asterisks).

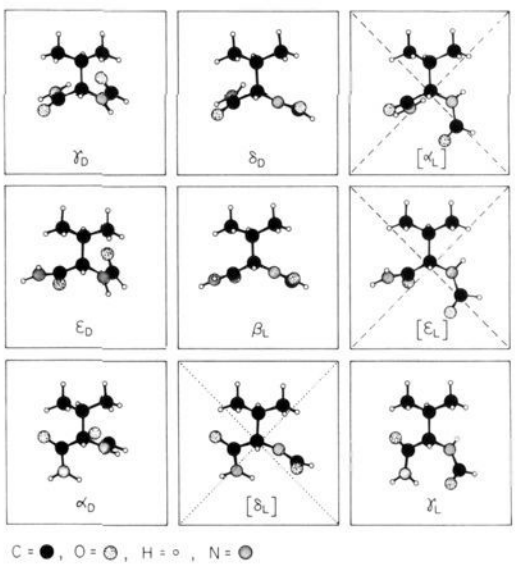

Figure 4. Molecular structures for a variety of backbone conformations of formyl-L-valinamide at $\chi^1 = 180°$ arranged according to the topology of the two-dimensional Ramachandran map. (The δ_L conformation disappears at $\chi^1 = 180°$; the structure shown is the starting point of the attempted geometry optimization.)

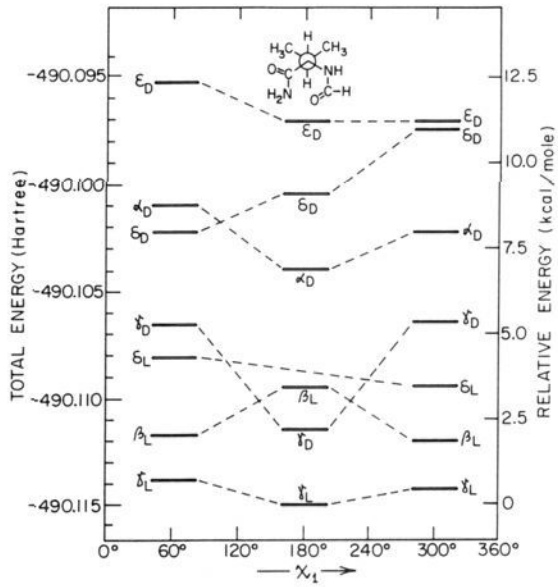

Figure 5. Energy level diagrams for the seven minima (α_D, β_L, γ_D, γ_L, δ_L, δ_D, ϵ_D) of the two-dimensional Ramachandran map as a function of χ^1.

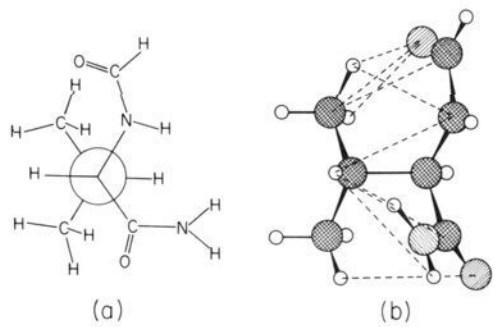

Figure 6. Molecular structure for the expected δ_L conformation at $\chi^1 = 180°$ for L-valineamide (the torsional angles ϕ and ψ are assumed to have the values of 60° and 180°, respectively): (a) Newman projection; (b) 3-D representation. Atom distances smaller than 3 Å are evidenced by dotted lines.

Chart IV

$\gamma_D\ \delta_D$ —	$\gamma_D\ \delta_D$ —	$\gamma_D\ \delta_D$ —
$\epsilon_D\ \beta_L$ —	$\epsilon_D\ \beta_L$ —	$\epsilon_D\ \beta_L$ —
$\alpha_D\ \delta_L\ \gamma_L$	α_D — γ_L	$\alpha_D\ \delta_L\ \gamma_L$
..$\chi^1 = 60^0$..	..$\chi^1 = 180^0$..	..$\chi^1 = 300^0$..

= 300°. For the remaining four backbone conformations (γ_L, γ_D, β_L, and α_D), the $\chi^1 = 180°$ (*anti*) conformation is either stabilized or destabilized with respect to the two nonequivalent *gauche* conformations ($\chi^1 = 60°$ and $\chi^1 = 300°$). Consequently, for most of the backbone conformations, whatever stabilizing or destabilizing effect the two CH_3 groups might have had in the $\chi^1 = 180°$ conformation, it is reduced in the $\chi^1 = 60°$ and $\chi^1 = 300°$ conformations. One must remember that, in contrast to the 180° conformation, in the 60° conformation the *anti* position of the C^β tertiary hydrogen is occupied by a CH_3, and in the 300° conformation the same position is occupied by another CH_3 group, while the two tertiary protons are *gauche*, in relation to each other, in both of the cases.

Considering now the annihilation of the minimum δ_L, observed on the two-dimensional potential energy surface corresponding to the *anti* ($\chi = 180°$) side-chain conformation, the structure corresponding to that precise combination of side-chain and backbone conformations is subjected to extra destabilizing factors. In other words, in the two *gauche* conformations such an effect is created by one methyl group only while in the *anti* conformation both methyl groups have these extra destabilizing factors, which are sufficiently large to annihilate the minimum. Note that such an effect is not operative for alanine. Due to the nature of the backbone folding in δ_L structures (Figure 6a), most of the atoms of the side chain in the $\chi = 180°$ conformation are found to be very close to the main chain atoms. In fact, it can be observed from Figure 6b that the distances between backbone and side-chain atoms are shorter than 3 Å in several cases. As a consequence, the critical point index λ (the number of negative eigenvalues of the force constants matrix) increases from $\lambda = 0$, characteristic for a minimum, to $\lambda = 1$, characteristic for a transition structure.

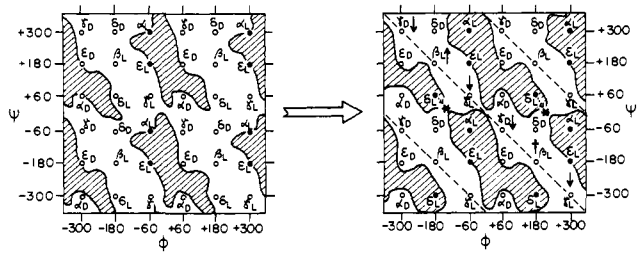

Figure 7. Schematic illustration of the anticipated change in the shape of the diagonal mountain ridge on the 2D Ramachandran map for For-Val-NH_2 as the ^{i}Pr group is rotated from $\chi^1 = 60°$ (left-hand side) to $\chi^1 = 180°$ (right-hand side). The asterisk illustrates that the δ_L conformation becomes a transition structure at $\chi^1 = 180°$.

The most puzzling phenomenon, as revealed by Figures 2 and 5, is the changing topology of the $E = E(\phi,\psi)$ PES as one rotates the ^{i}Pr group from $\chi^1 = 60°$ to $\chi^1 = 180°$ and finally to $\chi^1 = 300°$.

As can be seen from Chart IV as well as from Figure 2, the topology of the PES of valinediamide in its two *gauche* conformations ($\chi^1 = 60°$ and $\chi^1 = 300°$) is the same as the topology of alaninediamide published earlier.[10] Furthermore a detailed PES for the *anti* conformation ($\chi^1 = 180°$) of valinediamide would reveal that the mountain ridge that is roughly parallel to the principal diagonal (along the disrotatory mode of motion) does change its shape substantially with respect to the two *gauche* PES's. In the absence of such data, a schematic PES may be drawn to illustrate the changes strongly suggested by Figure 5 when the ^{i}Pr group is rotated to the *anti* conformation ($\chi^1 = 180°$). Such schematic surfaces are shown by Figure 7, which is constructed on the basis of Figure 12 of ref 26.

The $\chi^1 = 180°$ portion of Figure 7 shows the major features of Figure 5 that must be associated with the change of shape of this nearly diagonal mountain of the PES which represents repulsive interaction. (1) The mountain became narrower at its two ends, which led to the energy decrease of the γ_D and γ_L conformations. (2) The mountain became wider at its central part, which led to an energy increase of the β_L conformation. (3) The mountain became elongated, and that has changed the minimum, labeled as δ_L, to a first-order saddle point ($\lambda = 1$) denoted by *. Of course such a change can only occur within the previously recognized selection rules[27,28] involving the collapse of the minimum with two adjacent saddle points. This rule has been instrumental in explaining[10] the disappearance of the α_L and ϵ_L conformations.

It is also clear from Figure 7, just as Figure 5 suggested, that the most interesting region to investigate is along the principal diagonal (denoted by a broken line). This line, that passes through the γ_D, β_L, and γ_L conformations, is the most interesting because it includes the stabilized γ_D and γ_L conformations as well as the destabilized β_L conformation. These points are expected to be diagnostic of the change of shape of these diagonal mountain ridges which are entrenching this diagonal "grand canyon" denoted by a broken line.

3.3. Stabilization by Changing the Substituent and by Changing the Conformation: An Energy Partitioning. It can be suggested that there is a changing side chain/backbone interaction as the ^{i}Pr group is rotated about the C^α–C^β bond which assumes an extreme situation about $\chi^1 = 180°$. By analyzing the side chain/backbone interaction, using the quantitative analysis as described in the Methods section, it is hoped that some insights will be gained on the electronic mechanism of the PES modification which is caused by the rotation of the ^{i}Pr group. Tables II–V summarize the various numerical data obtained by such quantification.

The E_x^{stabil} values, compared for glycine-, alanine-, and valine-($\chi^1 = 180°$) diamides, are shown in Figure 8. While this figure shows some of the features of Figure 1, like the crossover of β_L and γ_D energy values on going from alanine- to valine- ($\chi^1 = 180°$) diamides, it also shows quite dramatically the stabilizing effect of the alkyl side chains. Furthermore, if one compares Figurds 1 and 8 with Figure 5, it becomes clear that the β_L/γ_D energy crossover is not really due to the change of Me to ^{i}Pr but to the rotation of the ^{i}Pr group from $\chi^1 = 60°$ or $\chi^1 = 300°$ to $\chi^1 = 180°$. It may then be useful to look at the energy components of the various backbone conformations for GLY (Table III) and for ALA (Table IV) and to compare them to the corresponding quantities for VAL (Table V) as a function of χ^1.

Table II. Total Energies of the Reference Fragments Minimized at the HF/3.2G Level of Theory

compounds	total energy[a]
CH_4	−39.976 877
H_3C–CH_3	−78.793 948
H_3C–$CH(CH_3)_2$	−156.434 471
H_2NCO–CH_2–$NHCHO$	−373.648 707

[a] hartrees.

Table III. Energy Components of E_x^{stabil} for For-Gly-NH_2

	backbone conformation[a]				
component[b]	α	β	γ	δ	ϵ
E_{dist}^{AH}	4.46	0.62	0.00	3.27	
E_{dist}^{RMe}	0.74	0.06	0.24	0.61	
E_{dist}^{HMe}	0.74	0.06	0.24	0.61	
E^{int}	0.00	0.00	0.00	0.00	
E_x^{stabil}	4.46	0.62	0.00	3.27	

[a] $\alpha = \alpha_D = \alpha_L$, $\beta = \beta_D = \beta_L$, $\gamma = \gamma_D = \gamma_L$, $\delta = \delta_D = \delta_L$, and $\epsilon = \epsilon_D = \epsilon_L$. See Chart Ia for details. [b] Energy components according to eq 12.

Table IV. Energy Components of E_x^{stabil} for For-L-Ala-NH_2 (kcal/mol)

	backbone conformation[a]						
component	α_D	β_L	γ_D	γ_L	δ_D	δ_L	ϵ_D
E_{dist}^{AH}	29.61	1.00	1.35	0.39	6.56	20.53	6.15
E_{dist}^{RMe}	37.90	0.41	0.97	0.37	0.41	34.62	0.58
E_{dist}^{HMe}	19.04	0.20	0.91	0.18	0.20	15.83	0.45
E^{int}	−48.17	−5.59	−4.51	−6.20	−5.17	−41.14	−3.73
E_x^{stabil}	0.30	−4.38	−3.10	−5.62	1.69	−1.82	2.55

[a] See Chart Ia for details. [b] Energy components according to eq 12.

Table V. Energy Components of E_x^{stabil} for For-L-Val-NH_2 (kcal/mol)

component[b]	α_D	β_L	γ_D	γ_L	δ_D	δ_L	ϵ_D
Backbone Conformations for $\chi^1 = 60°$ [a]							
E_{dist}^{AH}	9.03	2.10	4.39	1.41	7.62	4.83	8.21
E_{dist}^{RMe}	2.41	1.11	3.92	1.12	1.08	1.26	4.33
E_{dist}^{HMe}	1.52	0.41	2.25	0.69	0.42	0.78	0.86
E^{int}	−6.64	−6.23	−6.24	−6.59	−5.94	−6.49	−4.74
$E_{stabilX}$	3.28	−3.43	−0.18	−4.75	2.34	−1.18	6.94
Backbone Conformations for $\chi^1 = 180°$ [a]							
E_{dist}^{AH}	7.23	3.33	1.60	1.02	8.71		8.98
E_{dist}^{RMe}	1.20	0.84	0.93	0.37	0.58		0.84
E_{dist}^{HMe}	0.69	0.48	0.87	0.31	0.48		0.55
E^{int}	−6.40	−5.75	−4.84	−6.50	−5.21		−3.96
E_x^{stabil}	1.34	−2.07	−3.21	−5.41	3.60		5.31

[a] See Chart Ia for details. [b] Energy components according to eq 12.

(26) Perczel, A.; Viviani, W.; Csizmadia, I. G. Peptide Conformational Potential Energy Surfaces and Their Relevance to Protein Folding. In *Molecular Aspects of Biotechnology: Computational Models and Theories*; Bertran, J., Ed.; Kluwer Academic Publishers: Dordrecht, The Netherlands, 1992; pp 39–82.

(27) Mezey, P. G. *Potential Energy Hypersurfaces*; Elsevier Science Publishers: Amsterdam, The Netherlands, 1987; pp 227.

(28) Angyan, J. G.; Daudel, R.; Kucsman, A.; Csizmadia, I. G. *Chem. Phys. Lett.* **1987**, *136*, 1.

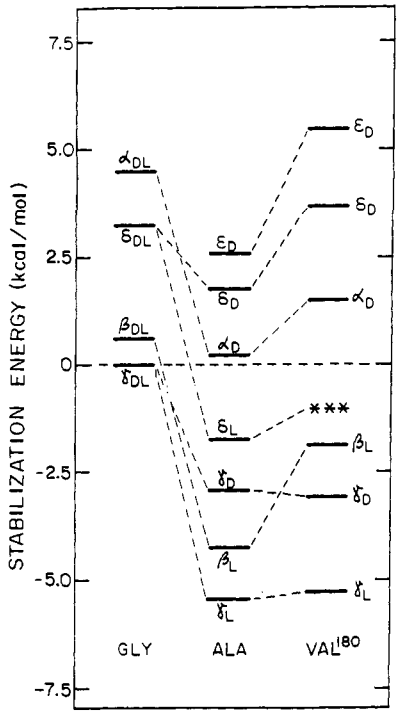

Figure 8. Comparison of stabilization energy E_x^{stabil} for the various backbone conformations of glycine, alanine, and valine derivatives. The symbol * * * denotes the anticipated position of the δ_L backbone conformation which was annihilated at the χ^1 = 180° side-chain conformation.

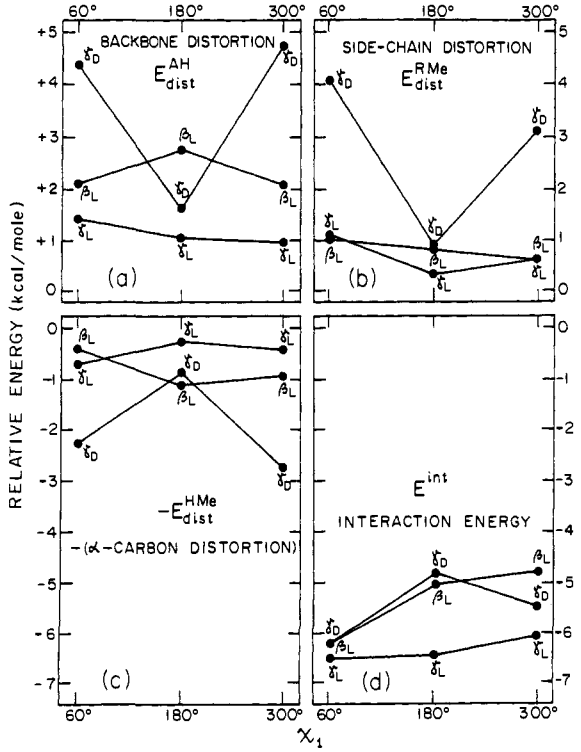

Figure 9. Comparison of the various distortion energies (E_{dist}^{AH}, E_{dist}^{MeR}, E_{dist}^{MeH}) and the sidechain/backbone interaction (E^{int}) for For-Val-NH_2 as a function of ^{i}Pr torsional angle χ^1 for the β_L, γ_L, and γ_D backbone conformations. The straight lines joining the points illustrate correspondance only and not linear variation.

The next question is how the components of the stabilization energy for valine are changing with χ^1. This data is presented graphically in Figure 9. The top two plots contribute by positive energy values and the bottom two plots contribute by negative

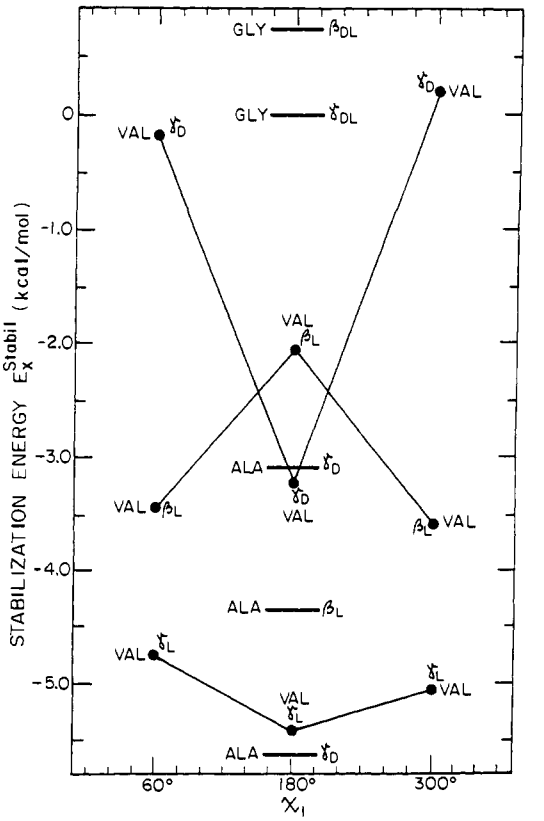

Figure 10. Comparison of the stabilization energy (E_x^{stabil}) of For-Val-NH_2 (VAL) as a function of ^{i}Pr torsional angle (χ^1) with the corresponding For-Gly-NH_2 (GLY) and For-Ala-NH_2 (ALA) values for the β_L, γ_L, and γ_D backbone conformations. The straight lines joining the points illustrate correspondence only and not linear variation.

Chart V

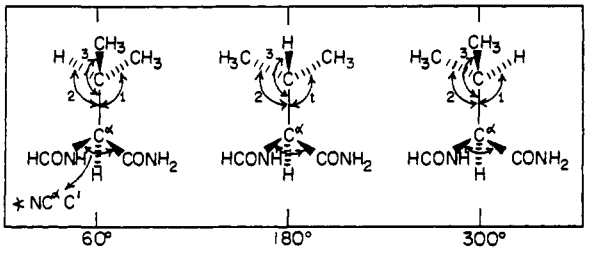

energy to the net stabilization energy E_x^{stabil}. (In this figure the quantity plotted is $-E_{dist}^{HMe}$ because this otherwise positive quantity enters with a minus sign in eq 9.)

On the basis of those diagrams (Figure 9), one may see that at χ^1 = 180° the determining component of the β_L net destabilization (Figure 10) is the backbone distortion (Figure 9a) while the net stabilization of γ_D (Figure 10) is dominated jointly by the backbone and the side-chain distortions (Figure 9a and b). This double enforcement is how the two *gauche* side-chain conformations of the γ_D backbone conformation are so destabilized and the *anti* conformation is stabilized. After relaxing these two less stable *gauche* side-chain conformations of γ_D to the *anti* side-chain conformation, on balance, there is a drop of over 3 kcal/mol in net stabilization. Yet, at this exact point, the backbone distortion alone contributes almost 1 kcal/mol destabilization to the net β_L destabilization, which is almost a net 1.5 kcal/mol (Figure 9), resulting in the β_L/γ_D energy crossover. This implies that the anomalous energetic behavior of the β_L conformation seen in Figure 5 resides almost exclusively in the energy change associated with the backbone distortion. This may then be seen as a tendency to increase the distance from the π electron density region of both acid-amide (CONH) moieties

Table VI. Selected Bond Angles of HCONH–CH(R)–$CONH_2$ for Varying Side Chains (R) as a Function of Conformational Change

BB[a] conf	bond angle	GLY (R = H)	ALA (R = Me)	VAL (R = iPr) $\chi^1 = 60°$ [b]	VAL (R = iPr) $\chi^1 = 180°$ [b]	VAL (R = iPr) $\chi^1 = 300°$ [b]
	1		110.15	110.10	109.92	106.03 (H)
	2		110.18	105.82 (H)	110.92	110.17
γ_L	3		110.16	113.49	107.96 (H)	113.12
	$NC^\alpha C'$	112.45	109.79	109.63	107.47	110.47
	1		109.51	112.52	110.88	107.08 (H)
	2		108.28	104.30 (H)	110.50	110.99
β_L	3		111.49	111.49	107.10 (H)	111.03
	$NC^\alpha C'$	107.75	106.36	105.64	105.57	106.79
	1		110.61	108.93	109.97	104.24 (H)
	2		109.61	105.81 (H)	109.78	110.07
γ_D	3		109.41	114.10	108.43 (H)	114.48
	$NC^\alpha C'$	112.45	113.57	116.22	112.13	117.36

[a] Backbone conformation. [b] Nominal torsional angle about the C^α–C^β bond.

to the isopropylic hydrogens. Conversely, in the case of γ_D conformation, the rotation of the side chain from $\chi^1 = 60°$ or $\chi^1 = 300°$ to $\chi^1 = 180°$ decreases the distance from both π electron clouds to the methyl hydrogen atoms of the *i*Pr group. This results in a decrease of the total distortion energy of the structure.

3.4. Influence of ^{i}Pr Group Rotation on the Steric Effect. Looking at the optimized geometrical parameters, the changes in bond lengths were rather small but some bond angles, adjacent to the C^α–C^β bond, did change appreciably with χ^1. Such an angular change may be used to monitor the change in steric interaction. We consider here the four bond angles (denoted by $NC^\alpha C'$, 1, 2, and 3) as depicted in Chart V.

Note that if the steric repulsion exerted by the ^{i}Pr group then is repelling the two peptide bonds, the angle labeled as $NC^\alpha C'$ is getting smaller. In contrast to that, if the two peptide bonds are pushing the ligands of the ^{i}Pr group, angles 1, 2, and 3 are expected to be larger.

The numerical data are summarized in Table VI and Figures 11 and 12. Looking at Figure 11 we can see that when the two CH_3 groups get close to the two peptide bonds at $\chi^1 = 180°$, the $NC^\alpha C'$ angle assumes a minimum value, indicating that the repulsive interaction is the greatest. However the backbone geometry change (Figure 10) and the backbone distortion energy change (Figure 9a) do not correlate in an obvious fashion, which is not true for the side-chain distortion energy curve (Figure 9b).

Considering Figure 12 we can see that the bond angle associated with environment 3 is minimum at $\chi^1 = 180°$, implying that the C^β–H bond, due to its small size, is not influenced greatly. However when the CH_3 group occupies environment 3 at $\chi^1 = 60°$ and 300°, bond angle 3 increases a great deal.

Considering angles 1 and 2 we can conclude from Figure 12 that these angles are the smallest when the hydrogen occupies these environments and considerably greater when the CH_3 groups occupy them. There appears to be no direct correlation between the variation of these bond angles (Figure 12) and the energy changes shown in Figure 10.

3.5. Effect of ^{i}Pr Group on Electron Distribution. Finally, it is worthwhile to return to the question of stabilization by the ^{i}Pr group. In a previous paper[24] we showed that the overall stabilization of the alanine derivative compared with the corresponding glycinediamide conformations was mainly due to induction (dipole–induced dipole interaction). In the case of the valine derivative, the induction effect, which is expected to be larger due to the greater average polarizability of the ^{i}Pr group, is partly canceled by steric hindrance. Nevertheless, one should keep in mind that the ^{i}Pr group exhibits an anisotropic polarizability which can be visualized by considering that the two methyl groups are more polarizable than the remaining H^β atom. Consequently, the inductive forces are χ^1 dependent, and the modulations of this contribution to the intramolecular energy can be analyzed by following the variation of charges as a function of χ^1 for each backbone conformation. Mulliken Population Analysis gives a rough but nevertheless useful idea in this respect.

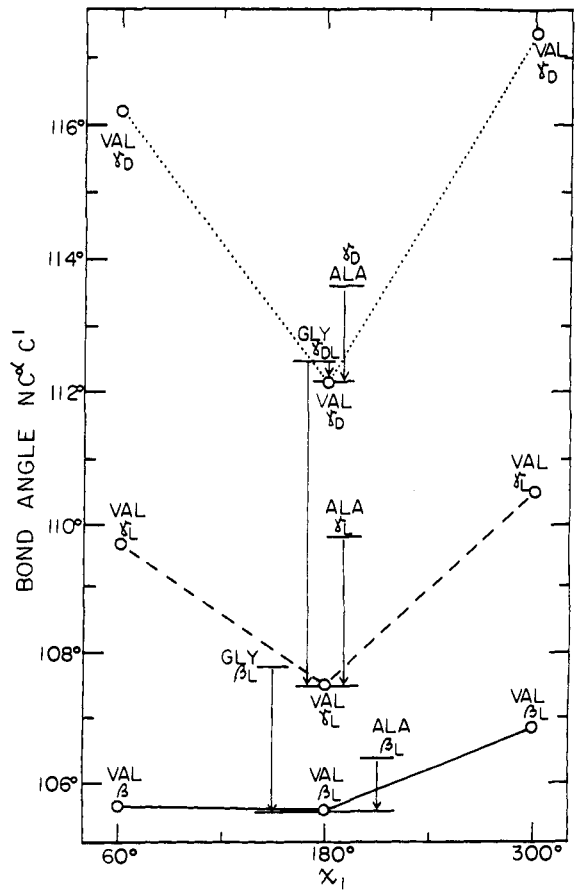

Figure 11. $NC^\alpha C'$ bond angle change with side-chain conformations of HCONH–CH(R)–$CONH_2$. The straight lines joining the points illustrate correspondance only and not linear variation.

This process is exemplified for the case of the γ_L conformation by the data given in Table VII, in which the charge of a CH_3 group is the sum of the four net atomic charges. The orientation of the backbone dipole moment is depicted as a vectorial sum of the moments of the two peptide bonds in Figure 13d. The induced dipole moment in the ^{i}Pr is expected to increase the positive charge of the group close to the negative end and *vice versa*. The induced moment is shown schematically by a broken arrow in Figure 13d. The dipole is oriented according to the chemical convention, pointing from the positive to the negative end.

The data in Table VII are in accordance with the role of induction and can explain the overall stabilization of $\chi^1 = 180°$ conformation with respect to the two *gauche* conformations.

4. Conclusions

Hitherto it was not so obvious that in peptides an apolar side chain may influence the relative orientation of the polar backbone

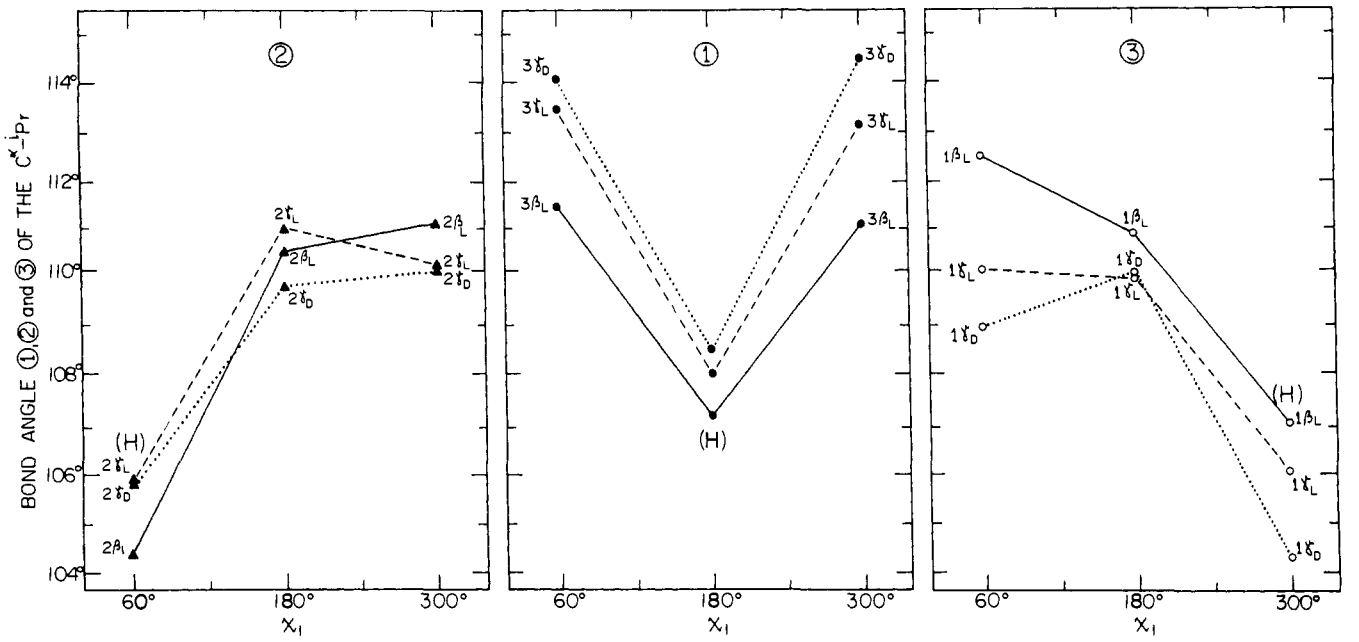

Figure 12. Variation of $C^{\alpha}C^{\beta}Q^{\prime}$ bond angles in the ^{i}Pr side chain for the γ_L, β_L, and γ_D backbone conformations of the valine derivative with side-chain torsional angle χ^1. The straight lines joining the points illustrate correspondance only and not linear variation.

Table VII. Results of Mulliken Population Analysis at the HF/3-21G Level of Theory for the γ_L Backbone Conformation of For-Val-NH_2

atom	$\chi^1 = 60°$	$\chi^1 = 180°$	$\chi^1 = 300°$
C4	−0.2989	−0.3149	−0.3057
H6	0.2268	0.2429	0.2570
$C5H_3$	0.0651	0.0505	0.0490
$C6H_3$	0.0512	0.0678	0.0508

amide groups very extensively. The *ab-initio* calculations reported here have proved that even an apolar bulky side chain is able to interact with a peptide backbone and could induce the annihilation of some otherwise legitimate minima through an unfavorable backbone and side-chain torsional angle combination. By contrast, the existing backbone minima are close to those previously found for glycine and/or alanine derivatives. As has been shown, all minima are located in one of the nine catchment regions[27] regardless of the type and/or orientation of the side chain. Therefore the annihilation of some backbone minima may occur due to an unfavorable side-chain conformation. It should be emphasized that we have never observed the creation of a new type of backbone minimum. Thus the recently published[10] nine type of legitimate backbone minima can still be regarded as an upper limit.

The quantification of side-chain and backbone contributions to the total energy gave us many useful insights that helped us to identify the electronic effects involved in conformational stability.

Even though the isopropyl side chain in most cases exhibits an extensive geometrical distortion, which is in fact a destabilization, the electronic stabilization of the ^{i}Pr group partially compensates for this, such that on balance, the final stability of valine is comparable to that of alanine.

The anisotropy of the ^{i}Pr compared to the methyl group generates three nonequivalent minimum-energy conformations in valine for each degenerate conformation of alanine. This χ^1 dependence can be explained by combined steric hindrance and dipole–induced dipole interaction contributions to the conformational energy.

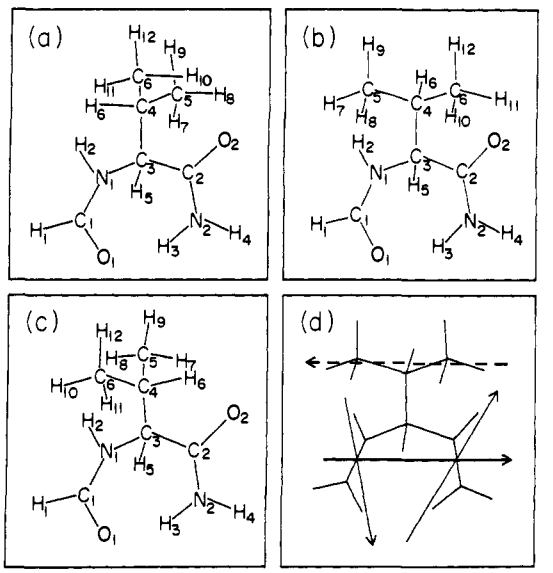

Figure 13. Atomic labels for For-Val-NH_2 (VAL) in its $\chi^1 = 60°$ (a), $\chi^1 = 180°$ (b), and $\chi^1 = 300°$ (c) side-chain conformations. The lower part of part d shows schematically the permanent dipole (horizontal solid arrow) as the vectorial sum of the two peptide bond dipoles (diagonal solid arrows). The upper part of part d shows schematically the side-chain dipole (broken arrow) induced in the opposite direction.

Acknowledgment. The *ab-initio* computations were carried out at CIRCE (Orsay, France). The authors thank IBM-France and CNRS for the generous allocation of computer time within the framework of the GS (Groupement Scientifique) "Modelisation Moléculaire". The continued financial support of the NSERC of Canada is gratefully acknowledged. This research was also supported in part by the Hungarian Scientific Research Foundation (OTKA no. III-2245).